



# Corrosion behaviour of NiCrFeAl-hBN seal coatings in oxidation environments at a high temperature

Su-Yuan Yang\* , Dan Guo, Xing-Wang Cheng, Jian-Ming Liu, Yue-Guang Yu

Received: 5 March 2019 / Revised: 9 May 2019 / Accepted: 29 May 2020 / Published online: 17 July 2020  
© The Nonferrous Metals Society of China and Springer-Verlag GmbH Germany, part of Springer Nature 2020

**Abstract** The purpose of this investigation was to evaluate the microstructure, high-temperature oxidation behaviour, and hardness of a seal coating under controlled exposures at 750 °C with different exposure times. The results reveal that the main phases in the coating are Ni, FeNi<sub>3</sub>, and hexagonal BN, with  $\alpha$ -Al<sub>2</sub>O<sub>3</sub> peaks appearing after 2-h oxidation. As the exposure time increases, the diffraction peak intensity of  $\alpha$ -Al<sub>2</sub>O<sub>3</sub> begins to decrease and Cr<sub>2</sub>O<sub>3</sub> peaks appear after 200 h. After 1000 h, Cr<sub>2</sub>O<sub>3</sub> becomes dominant with only small amounts of  $\alpha$ -Al<sub>2</sub>O<sub>3</sub> remaining. The high-temperature oxidation process of the coating includes three stages: the fast stage, transition stage, and slow stage. The oxidation rate is constant in each stage, and in the fast stage and slow stages with values of  $7.59 \times 10^{-4}$  and  $8.37 \times 10^{-5} \text{ mg}^2 \cdot \text{cm}^{-4} \cdot \text{s}^{-1}$ , respectively. Initially,  $\alpha$ -Al<sub>2</sub>O<sub>3</sub> forms near the pores in the coating, followed by the formation of Cr<sub>2</sub>O<sub>3</sub>. As the exposure time increases, oxidation penetrates into the interior of the coating along phase boundaries to form island-shaped inner oxide layers with high concentrations of Cr, Ni, and Fe. Additionally, hardness increases with increasing oxide percentage.

**Keywords** NiCrFeAl-hBN; Seal coating; Oxidation; Microstructure; High temperature

## 1 Introduction

With the rapid development in the aviation industry, large propulsive force, high efficiency, and low fuel consumption have become the main objectives of the design and manufacture of aircraft engines [1, 2]. However, the gap between engine blades and the engine casing is an important factor that reduces the overall efficiency of an engine and increases fuel consumption [3, 4]. Based on various factors, such as thermal expansion of the engine assembly and elongation of the blades caused by high-speed rotational centrifugal force, this gap cannot be controlled to zero [5, 6]. Therefore, abradable seal coatings are deposited onto the shrouds aircraft engines using thermal spray technology to minimize blade-tip clearances and enhance the efficiency of engines. Such coatings have many advantages, such as simple manufacturing processes, easy to repair, adjustable properties, and good sealing effectiveness [7]. Abradable seal coatings operate in highly demanding environments and are required to exhibit certain properties, including abradability, corrosion resistance, high-temperature stability, erosion resistance, and sufficient bond strength with the underlying material [8–10]. To meet this complex combination of requirements, such coatings are largely composed of metal phases (e.g., Ni, Cu, Al, and various alloys) and self-lubricating non-metal phases (e.g., graphite, hBN diatomite, and high molecular polymers) with high porosity [11]. Metal phases provide high strength, oxidation resistance, and hot-corrosion resistance. Self-lubricating non-metal phases mainly provide lubrication for coatings and enhance porosity to reduce the hardness of coatings [12, 13].

Su-YuanYang\*, D. Guo, X.-W. Cheng  
School of Materials Science and Engineering, Beijing Institute of Technology, Beijing 100081, China  
e-mail: yangsuyuan@bit.edu.cn

Su-YuanYang, X.-W. Cheng  
National Key Laboratory of Science and Technology on Materials Under Shock and Impact, Beijing 100081, China

J.-M. Liu, Y.-G. Yu  
Beijing General Research Institute of Mining and Metallurgy, Beijing 100160, China

The structures and properties of thermally sprayed coatings depend heavily on their level of oxidation, which is one of the key characteristics of such coatings. The working environment of a seal coating is a high-temperature oxidation atmosphere and oxidation is one of the main failure modes of such coatings. Therefore, it is important to study the microstructure changes in seal coatings after exposure to a high temperature to research this failure process and improve service life [14–17].

However, most previous studies have focused on other properties, such as abrasability and anti-erosion ability [18–22], meaning fundamental investigations of microstructure and thermal properties are still lacking [23, 24]. In this study, the microstructure and high-temperature oxidation behaviours of a NiCrFeAl-hBN seal coating were investigated at 750 °C with various exposure times.

## 2 Experimental

The seal coating system studied in this work (Fig. 1a) consists of a GH4169 substrate, APS-deposited NiCrAl bond coating, and NiCrFeAl-hBN top coating (~ 1.5 mm in thickness) that was applied using a flame spray process (Table 1). The feedstock powders for the top coating were supplied by Beijing General Research Institute of Mining and Metallurgy (China). Their chemical compositions are listed in Table 2. The size of the top coating powders was relatively uniform, as shown in Fig. 1b. The NiCrAl powders were pre-sprayed onto the surface of the GH4169 substrate to a thickness of ~ 60 µm to improve the adhesive bond strength of the seal coating.

The coated specimens were treated at 750 °C in an ambient atmosphere with exposure times of 2, 6, 40, 80, 200, and 1000 h, and then cooled in open air. The oxidized samples were subjected to a discontinuous weighing method. Specifically, after a certain period of oxidation, the

**Table 1** Process parameters of flame spraying

O <sub>2</sub> flow rate/ (m <sup>3</sup> ·h <sup>-1</sup> )	C <sub>2</sub> H <sub>2</sub> flow rate/ (m <sup>3</sup> ·h <sup>-1</sup> )	Powder feeding rate/(g·min <sup>-1</sup> )	Spraying distance/mm
1.2	0.9	40	200

**Table 2** Chemical composition of powders of NiCrFeAl-hBN top coating (wt%)

Elements	Ni	Cr	Fe	Al	BN
Content	Bal.	11–16	6–10	2.5–4.5	4.8–5.6

samples were cooled and weighed, then returned to the furnace for further oxidation, then cooled and weighed again. The samples were weighed by an electronic balance with an accuracy of 0.1 mg.

The microstructures of the NiCrFeAl-hBN coatings were investigated before and after high-temperature oxidation by means of scanning electron microscopy (SEM, FEI QUANTA 600) equipped with energy-dispersive spectroscopy (EDS), electron probe micro-analysis (EPMA, JXA-8230) compositional mapping, and X-ray diffraction (XRD, D8 advance) using a Cu K $\alpha$  radiation source. The volumetric porosity and oxide percentage of the top coat were determined by using an image analysis technique with the aid of the ImageJ software package. Hardness measurements were carried out for all specimens by using an HR15Y device (MODEL 600 MRD-S).

## 3 Results and discussion

### 3.1 Phase analysis

XRD patterns of the coatings treated at 750 °C for 0, 2, 200, and 1000 h are presented in Fig. 2. The main phases

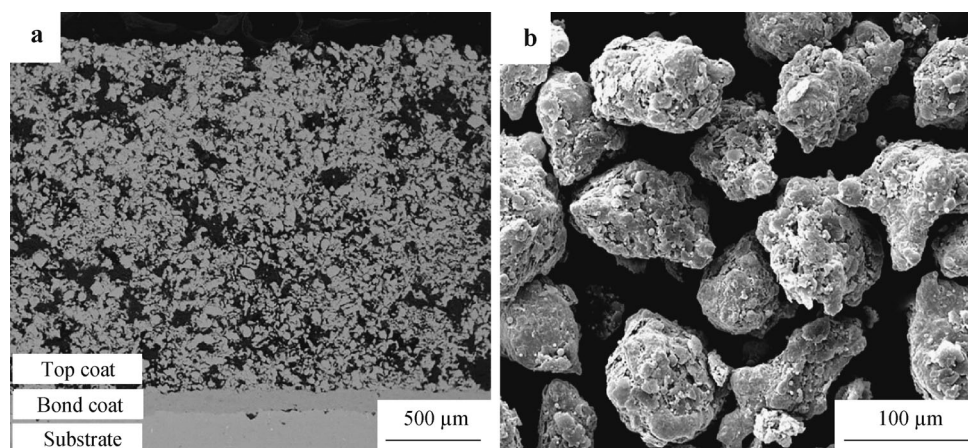


**Fig. 1** SEM images of **a** abrasible seal coating and **b** powders

in the untreated coating were Ni, FeNi<sub>3</sub> and hexagonal BN. After 2-h exposure at 750 °C,  $\alpha$ -Al<sub>2</sub>O<sub>3</sub> peaks appeared in the diffraction pattern, indicating that the oxidation of aluminium occurred during the exposure process. As the exposure time increased, the diffraction peak intensity of  $\alpha$ -Al<sub>2</sub>O<sub>3</sub> began to decrease and Cr<sub>2</sub>O<sub>3</sub> peaks appeared after 200 h. After 1000 h, the oxide phase of Cr<sub>2</sub>O<sub>3</sub> became dominant, with only a small amount of  $\alpha$ -Al<sub>2</sub>O<sub>3</sub> remaining.

### 3.2 Microstructure

SEM microstructures of the coatings exposed at 750 °C for different exposure times are presented in Fig. 3. The

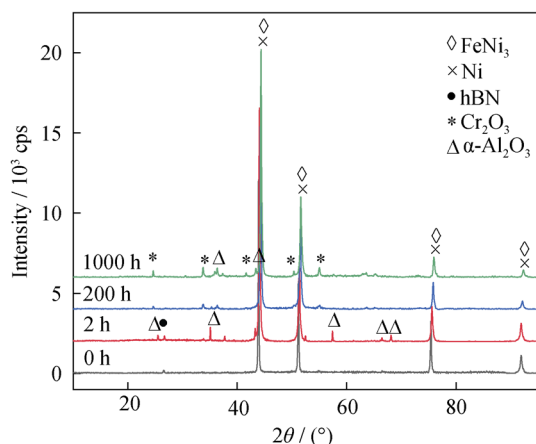


**Fig. 2** XRD patterns of NiCrFeAl-hBN coatings after exposure for different times at 750 °C

coatings are largely composed of hBN phases (dark grey) of varying size, metal matrices (white), and oxides (light grey) with significant levels of porosity (black). The chemical compositions of these regions were determined via EDS.

A summary of the compositional data of the points shown in Fig. 3 is provided in Table 3. The main elements in the light grey area are Al (exposure time  $\geq$  2 h) and Cr (exposure time  $>$  6 h). This result is supported by XRD results (Fig. 2). After heat treatment for 2 and 6 h (Fig. 3a, b, respectively), the oxides were largely composed of  $\alpha$ -Al<sub>2</sub>O<sub>3</sub>. When the heat treatment time was 40 and 80 h (Fig. 3c, d, respectively), the oxides were  $\alpha$ -Al<sub>2</sub>O<sub>3</sub> and Cr<sub>2</sub>O<sub>3</sub>. When comparing SEM images of these two oxides, the image of  $\alpha$ -Al<sub>2</sub>O<sub>3</sub> was found to be smoother than that of Cr<sub>2</sub>O<sub>3</sub>, as shown in Fig. 3c. After 200 h (Fig. 3e, f), Ni and Fe began to oxidize, but only to a small degree, so Fig. 2 does not show any peaks for these oxides. The oxides mainly appeared near the pores in the coating when the exposure time was short. After 200 h (Fig. 3f), oxides formed in the metal matrices. The oxides of Ni and Fe in the coating after 1000 h were more prominent than those in the coating after 200 h.

EPMA elemental mapping graphs for the NiCrFeAl-hBN coating after 2- and 1000-h oxidation at 750 °C are presented in Figs. 4 and 5, respectively. It is difficult to observe the existence of hBN using XRD or SEM due to its low content, but EPMA proves the existence of hBN. Although the content of hBN is low, its distribution is uniform (Figs. 4e and 5e), which ensures the abrasability

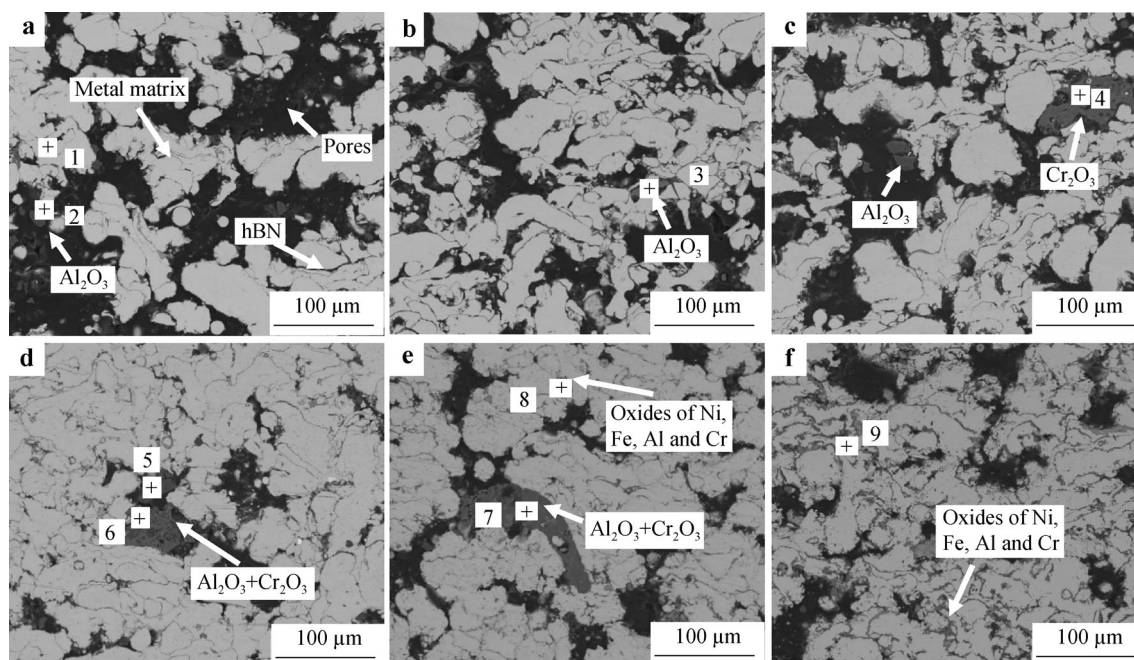


**Fig. 3** SEM images of NiCrFeAl-hBN coatings after different exposure times at 750 °C: **a** 2 h, **b** 6 h, **c** 40 h, **d** 80 h, **e** 200 h, and **f** 1000 h



**Table 3** Summary of EDS results for areas in Fig. 3 (at%)

Points	Ni	Cr	Fe	Al	O
1	73.17	17.10	9.73	–	–
2	–	–	–	57.67	42.33
3	–	–	–	60.77	39.23
4	–	24.35	–	11.14	64.51
5	–	–	–	60.37	39.63
6	–	35.17	–	19.25	45.58
7	–	27.25	–	15.44	56.11
8	23.43	19.44	1.39	10.05	45.69
9	32.06	17.69	6.21	1.78	42.27

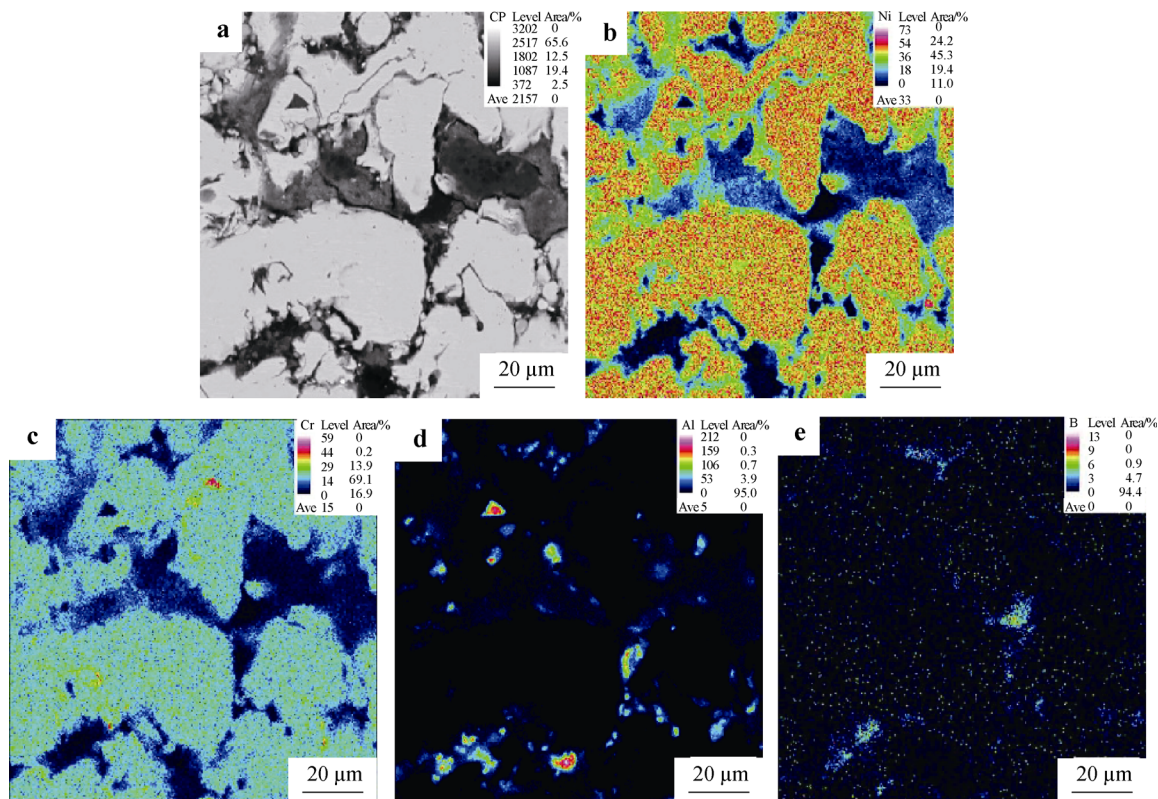
of the coating. Ni is the most abundant metallic element in the coating and mainly exists in metal matrices surrounded by Cr (Figs. 4b and 5b). As shown in Figs. 4d and 5d, Al mainly exists in the grey area around the pores (dark area). As shown by the results of XRD and SEM, it mainly exists in the form of  $\alpha$ -Al<sub>2</sub>O<sub>3</sub>. Cr is well distributed in the metal matrices after 2-h oxidation (Fig. 4c). After 1000 h, it largely exists around  $\alpha$ -Al<sub>2</sub>O<sub>3</sub> in the form of Cr<sub>2</sub>O<sub>3</sub>. Additionally, visible segregation of Cr in the metal matrices of the coating appears after 1000 h (Fig. 5c), which is considered to be the result of the long exposure time at 750 °C [25].

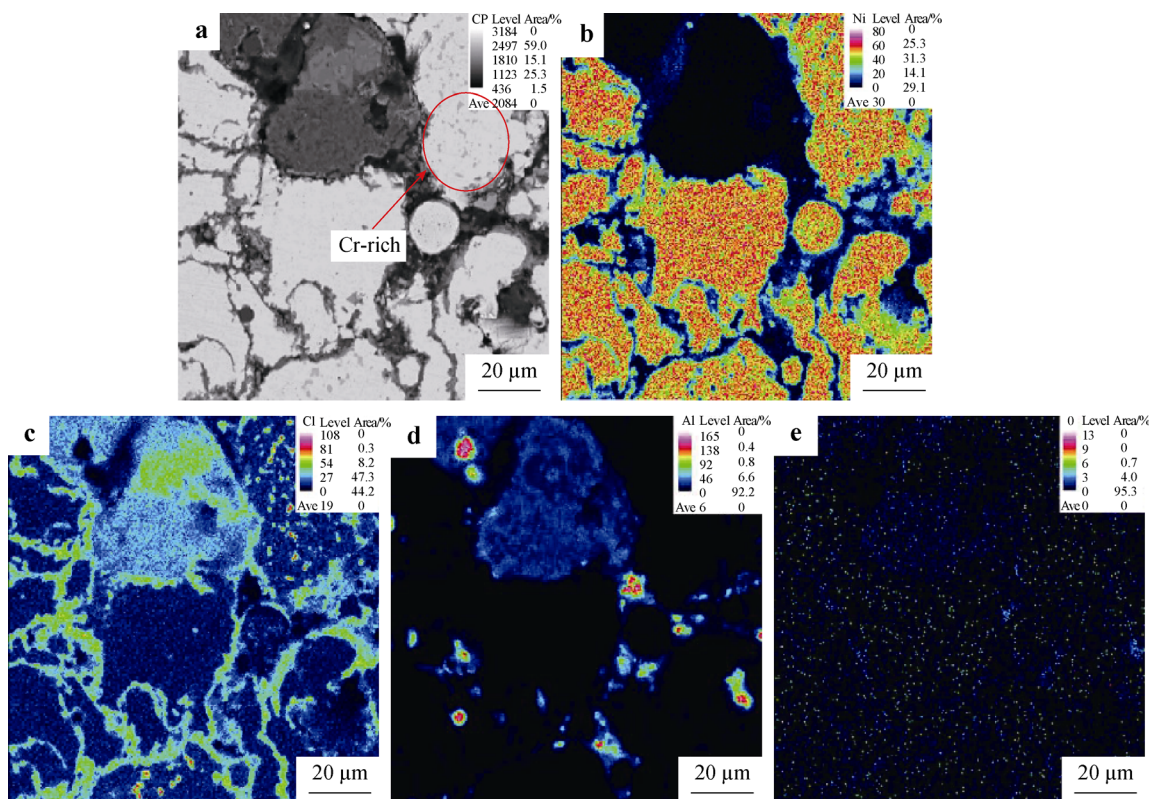
### 3.3 Porosity and oxide percentage

Figure 6 presents the changes in porosity and oxide content of the seal coatings with various exposure times at 750 °C. The porosity of the coating is approximately 23.5% without any heat treatment. This value decreases with prolonged exposure time, reaching 11.75% after 1000 h. The rate of decrease is rapid initially and then slows after 200 h. The oxide content in the coating increases with exposure time increasing. The main reason for the decrease in porosity over time is the change in the oxide percentage.

### 3.4 Oxidation kinetics

The oxidation weight change per unit area ( $\text{mg}\cdot\text{cm}^{-2}$ ) of the NiCrFeAl-hBN coating with heat treatment at 750 °C is presented in Fig. 7a. The oxidation weight change of the coating exhibits three main stages: the fast oxidation stage (0–30 h), transition stage, and slow oxidation stage (after 60 h). Figure 7b presents the square of the weight gain per unit area of the NiCrFeAl-hBN coating versus time. The fast and slow oxidation stages conform to the parabolic law, meaning that the oxidation dynamic parabola constant can be used to evaluate the oxidation rate. The oxidation rate constant ( $K_p$ , parabolic rate constant) was calculated by using a linear least-square function:

**Fig. 4** EPMA elemental mapping graphs for NiCrFeAl-hBN coating treated after 2 h at 750 °C **a** cp, **b** Ni, **c** Cr, **d** Al, and **e** B



**Fig. 5** EPMA elemental mapping graphs for NiCrFeAl-hBN coating treated after 1000 h at 750 °C **a** cp, **b** Ni, **c** Cr, **d** Al, and **e** B

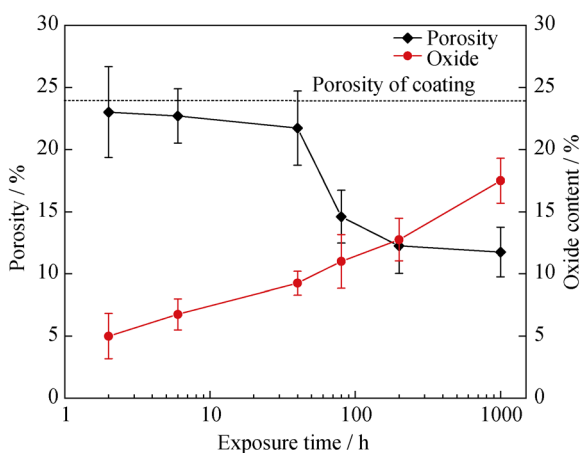


**Fig. 6** Curves of porosity and oxide percentage of coating versus exposure time at 750 °C

$$(\Delta W/A)^2 = K_p \times t \quad (1)$$

where  $(\Delta W/A)$  is the weight gain per unit area and  $t$  is the oxidation time in seconds [26]. The parabolic rate constants for the NiCrFeAl-hBN coating in the fast and slow oxidation stages are  $7.59 \times 10^{-4}$  and  $8.37 \times 10^{-5} \text{ mg}^2 \cdot \text{cm}^{-4} \cdot \text{s}^{-1}$ , respectively. The oxidation rate in the fast oxidation stage is an order of magnitude greater than that in the slow oxidation stage. Additionally, the oxidation rate constant in the fast

oxidation stage is approximately three orders of magnitude smaller than that of the substrate metal (GH4169), meaning that the NiCrFeAl-hBN coating successfully protects the substrate at high temperatures [27].

The metal elements in the coating largely consist of Ni, Cr, Fe, and Al, which can be oxidized into NiO,  $\text{Cr}_2\text{O}_3$ , FeO,  $\text{Fe}_2\text{O}_3$ ,  $\text{Fe}_3\text{O}_4$ , and  $\text{Al}_2\text{O}_3$  at 750 °C in air. The formula for Gibbs free energy ( $\Delta G_T$ ) is shown in Eq. (2).

$$\Delta G_T = \Delta G_0 + RT \ln \left( \frac{a_{\text{M}_x\text{O}_y}^2}{a_{\text{M}}^x a_{\text{O}_2}^y} \right), \quad (2)$$

where  $\Delta G_0$  is the change in metal oxidation free energy in the standard state ( $T = 298.15 \text{ K}$ ,  $p = 101.3 \text{ kPa}$ ,  $R = 8.314 \text{ J} \cdot \text{mol}^{-1} \cdot \text{K}^{-1}$ ), and  $a$  is the activity of the individual components.

When comparing the Gibbs free energies of the oxidized metal elements in the coating, we find that  $\Delta G_{\text{Al}_2\text{O}_3} < \Delta G_{\text{FeO}} < \Delta G_{\text{Fe}_3\text{O}_4} < \Delta G_{\text{Fe}_2\text{O}_3} < \Delta G_{\text{NiO}}$ . Therefore, Al is oxidized preferentially near the pores in the coating, followed by Cr. The high stability of these elements means that the Ni and Fe in the coating can be prevented from oxidizing during heat treatment. Furthermore, even if Ni and Fe are oxidized in the presence of Al and Cr, the oxides of Ni and Fe will become unstable and decompose back into Ni and Fe [28]. This is why no oxidation of Ni and Fe occurred in the coatings with short exposure time, as shown

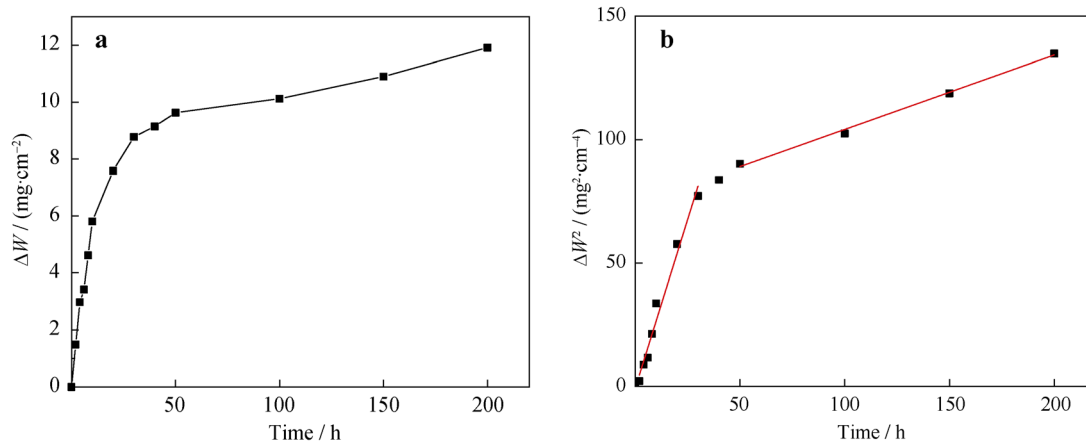


**Fig. 7** **a** Oxidation kinetics curve of NiCrFeAl-hBN coating at 750 °C; **b** relationship between square of weight gain and time of NiCrFeAl-hBN coating at 750 °C

in Figs. 2 and 3. After 200 h, based on the limited concentration of free Al and Cr, Ni and Fe begin to oxidize in the metal matrices. However, the peaks of Ni and Fe oxides cannot be observed in the XRD results, indicating low concentrations of these oxides.

With a further increase in the exposure time, additional oxygen ions diffuse into the interior of the coating through pores. Based on the large amount of defects at grain boundaries, high oxygen concentrations and low aluminium concentrations form deficient  $\text{Al}_2\text{O}_3$  to prevent further oxidation. However, oxidation develops in the interior of the coating along grain boundaries or phase boundaries to form island-shaped inner oxide layers. The formation and development of oxides along boundaries lead to the diffusion of Cr in the matrices into oxides, which reduces the concentration of Cr in the matrices [29]. This results in an uneven composition, and the inner oxide layer is enriched by higher Cr concentrations (Fig. 5c).

The weight gains of the coatings at 750 °C exhibit three stages because of the formation of oxides in the NiCrFeAl-hBN coating, as described above. In the fast oxidation stage, the main oxidation in the coating is the formation of  $\text{Al}_2\text{O}_3$ . Next,  $\text{Cr}_2\text{O}_3$  appears and oxides form around pores, where the chance to bond with oxygen atoms is sufficient. Based on the protection of these oxides, with oxidation time increasing, oxidation develops in the interior of the coating along grain boundaries or phase boundaries, where the chance of metal elements attaching to oxygen atoms is lower than that in the pores. The oxidation rate then slows and the process passes through the transition stage before reaching the slow oxidation stage. The growth rate of each oxide obeys parabolic kinetics, resulting in parabolic oxidation kinetics for the coating in each stage of oxidation [30–32].

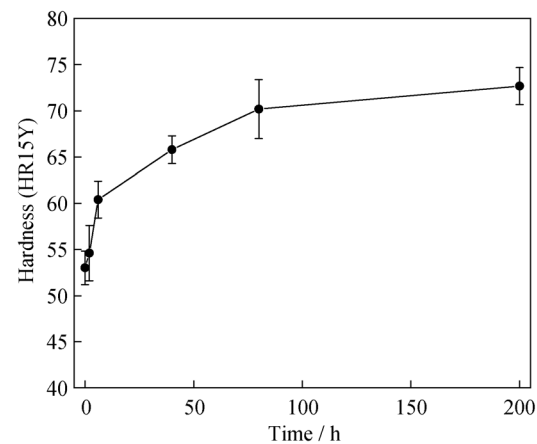


**Fig. 8** Curve of hardness of coatings versus exposure time at 750 °C

### 3.5 Hardness

Figure 8 presents the change in the hardness of NiCrFeAl-hBN seal coatings with various exposure time at 750 °C. One can see that the hardness increases as the heat treatment time increases. Furthermore, the rate of increase is rapid initially and then slows after 200 h. This phenomenon can be explained by the following reasons. First, the formation of oxides increases hardness because the hardness values of metal oxides, such as alumina and chromium oxide, are greater than those of the base metals. Second, previous studies have shown that the hardness of seal coatings can be affected by the changes in porosity [3, 8].

## 4 Conclusions

The microstructures and high-temperature corrosion behaviours of coatings under controlled exposure at 750 °C



with exposure time of 2, 6, 40, 80, 200, and 1000 h were investigated. The main results are as follows. The coating microstructure is composed of FeNi<sub>3</sub>, Ni, and hBN. The high-temperature oxidation process includes three stages: the fast stage, transition stage, and slow stage.  $\alpha$ -Al<sub>2</sub>O<sub>3</sub> peaks appear after 2-h exposure. As exposure time increases, the diffraction peak intensity of  $\alpha$ -Al<sub>2</sub>O<sub>3</sub> begins to decrease and Cr<sub>2</sub>O<sub>3</sub> peaks appear after 200 h. After 1000 h, Cr<sub>2</sub>O<sub>3</sub> becomes dominant with a small amount of remaining  $\alpha$ -Al<sub>2</sub>O<sub>3</sub>. The main oxides of  $\alpha$ -Al<sub>2</sub>O<sub>3</sub> and Cr<sub>2</sub>O<sub>3</sub> are formed around the pores in the coating initially. The inner oxide layer is enriched with higher concentrations of Cr, Ni, and Fe after 200 h. Finally, the hardness of the coating increases with exposure time increasing.

**Acknowledgments** This study was financially supported by the National Natural Science Foundation of China (No. 51571031).

## References

- [1] Yi M, He J, Huang B, Zhou H. Friction and wear behaviour and abrasibility of abrasible seal coating. *Wear*. 1999;231(1):47.
- [2] DeMasi-Marcin JT, Gupta DK. Protective coatings in the gas turbine engine. *Surf Coat Technol*. 1994;68:1.
- [3] Ma X, Matthews A. Investigation of abrasible seal coating performance using scratch testing. *Surf Coat Technol*. 2007;202(4):1214.
- [4] Siddiqui SM, Joshi P, Nayak N, Vidyasagar K. Thermal spraying, optimization and characterization of abrasible seal coating for gas turbine for service temperature up to 750 °C. *Adv Mater Lett*. 2014;5:506.
- [5] Taylor TA, Thompson BW, Aton W. High speed rub wear mechanism in IN-718 vs. NiCrAl-bentonite. *Surf Coat Technol*. 2007;202(4):698.
- [6] Wang J, Zhou Y, Chong XY, Zhou R, Feng J. Microstructure and thermal properties of a promising thermal barrier coating: YTaO<sub>4</sub>. *Ceram Int*. 2016;42(12):13876.
- [7] Zhang F, Xu CG, Lan H, Huang CB, Zhou Y, Du LZ, Zhang WG. Corrosion behavior of an abrasible seal coating system. *J Therm Spray Technol*. 2014;23(6):1019.
- [8] Faraoun HI, Grosdidier T, Seichepine JL, Goran D, Aourag H, Coddet C, Zwick J, Hopkins N. Improvement of thermally sprayed abrasible coating by microstructure control. *Surf Coat Technol*. 2006;201(6):2303.
- [9] Liu JM, Yu YG, Liu T, Cheng XY, Shen J, Li CH. The influence of composition and microstructure on the abrasibility of aluminum-based abrasible coatings. *J Therm Spray Technol*. 2017;26(6):1095.
- [10] Yu FL, Yu B, Wu XY, Wang HJ, Wu JH. Corrosion resistance and anti-wear property of nickel based abrasible sealing coating deposited by plasma spraying. *J Inorg Mater*. 2016;31(7):687.
- [11] Johnston R. Mechanical characterisation of AlSi-hBN, NiCrAl-bentonite, and NiCrAl-bentonite-hBN freestanding abrasible coatings. *Surf Coat Technol*. 2011;205(10):3268.
- [12] Johnston RE, Evans WJ. Freestanding abrasible coating manufacture and tensile test development. *Surf Coat Technol*. 2007;202(4):725.
- [13] Faraoun HI, Seichepine JL, Coddet C, Aourag H, Zwick J, Hopkins N, Sporer D, Hertter M. Modelling route for abrasible coatings. *Surf Coat Technol*. 2006;200(22–23):6578.
- [14] Soltani R, Heydarzadeh-Sohi M, Ansari M, Afsari F, Valefi Z. Effect of APS process parameters on high-temperature wear behavior of nickel-graphite abrasible seal coatings. *Surf Coat Technol*. 2017;321:403.
- [15] Ma X, Matthews A. Evaluation of abrasible seal coating mechanical properties. *Wear*. 2009;267(9):1501.
- [16] Rapp RA, Douglass DL. High temperature corrosion in energy systems. *Mater Sci Eng*. 1981;50(1):1.
- [17] Peng XM, Wu AR, Dong LJ, Tao YR, Gao WG, Zhou XL. Stability analysis of NiCrAlY coating/titanium alloy system under pure thermal exposure. *Rare Met*. 2017;36(8):659.
- [18] Stringer J, Marshall MB. High speed wear testing of an abrasible coating. *Wear*. 2012;294–295:257.
- [19] Delebarre C, Wagner V, Paris JY, Dessein G, Denape J, Gurt-Santanach J. An experimental study of the high speed interaction between a labyrinth seal and an abrasible coating in a turbo-engine application. *Wear*. 2014;316(1–2):109.
- [20] Cheng XD, Xiang HY, Ye WP, Meng XM, Min J, Liu MZ, Zhang P, Lu W. Effect of coated PHB on properties of abrasible seal coating. *J Wuhan Univ Technol Mater Sci Ed*. 2014;29(3):417.
- [21] Zhang N, Shen J, Xuan HJ, Hu YQ, Hong W. Evaluation of an AlSi-polyester abrasible seal coating performance using high-temperature and high-velocity abrasion tests. *Proc Inst Mech Eng Part J J Eng Tribol*. 2015;230(7):842.
- [22] Sampath S, Jiang XY, Matejcek J, Prchlik L, Kulkarni A, Vaidya A. Role of thermal spray processing method on the microstructure, residual stress and properties of coatings: an integrated study for Ni-5 wt%Al bond coats. *Mater Sci Eng, A*. 2004;364(1–2):216.
- [23] Han T, Xu X, Ge X, Zhong Y, Liu Q, Chen T. High temperature oxidation behavior of Ti-8Si-1.4-Zr-xY<sub>2</sub>O<sub>3</sub> alloy. *Chin J Rare Met*. 2018;42(02):130.
- [24] Li DQ, Zhou LX, Zhu KJ, Gu J, Zheng SH. Isothermal oxidation behavior of scandium and yttrium co-doped B2-type iron-aluminum intermetallics at elevated temperature. *Rare Met*. 2018;36(8):690.
- [25] Somasundaram B, Kadoli R, Ramesh MR. Evaluation of cyclic oxidation and hot corrosion behavior of HVOF-sprayed WC-Co/NiCrAlY coating. *J Therm Spray Technol*. 2014;23(6):1000.
- [26] Osorio JD, Hernández-Ortiz JP, Toro A. Microstructure characterization of thermal barrier coating systems after controlled exposure to a high temperature. *Ceram Int*. 2014;40(3):4663.
- [27] Uusitalo MA, Vuoristo PMJ, Mäntylä TA. High temperature corrosion of coatings and boiler steels in reducing chlorine-containing atmosphere. *Surf Coat Technol*. 2003;346(1):168.
- [28] Oksa M, Metsäjoki J. Optimizing NiCr and FeCr HVOF coating structures for high temperature corrosion protection applications. *J Therm Spray Technol*. 2014;24(3):436.
- [29] Ahmad B, Fox P. STEM Analysis of the transient oxidation of a Ni-20Cr alloy at high temperature. *Oxid Met*. 1999;52(1–2):113.
- [30] Chen JH, Rogers PM, Little JA. Oxidation behavior of several chromia-forming commercial nickel-base superalloys. *Oxid Met*. 1997;47(5–6):381.
- [31] An TF, Guan HR, Sun XF, Hu ZQ. Effect of the  $\theta$ - $\alpha$ -Al<sub>2</sub>O<sub>3</sub> Transformation in scales on the oxidation behavior of a nickel-base superalloy with an aluminide diffusion coating. *Oxid Met*. 2000;54(3–4):301.
- [32] Lin TY, Zhang XY, Huang X, Gong XP, Zhang JJ, Hu XJ. Microstructure and properties of microarc oxidation coating formed on aluminum alloy with compound additives nano-TiO<sub>2</sub> and nano-ZnO. *Rare Met*. 2018;36(11):976.